Reduced order modelling numerical homogenization

Assyr Abdulle[1], Yun Bai[1]

January 29, 2014

Abstract

A general framework to combine numerical homogenization and reduced order modeling techniques for partial differential equations (PDEs) with multiples scales is described. Numerical homogenization methods are usually efficient to approximate the effective solution of PDEs with multiple scale. However, classical numerical homogenization techniques require the numerical solution of a large number of so-called micro problems to approximate the effective data at selected grid points of the computational domain. Such computation become particularly expensive for high-dimensional, time-dependent or nonlinear problems. In this paper we explain how numerical homogenization method can benefit from reduced order modeling techniques that allow to identify offline and online computational procedures. The effective data are only computed accurately at a carefully selected number of grid points (offline stage) appropriately "interpolated" in the online stage resulting in a online cost comparable to a single scale solver. The methodology is presented for a class of PDEs with multiple scales, including elliptic, parabolic, wave and nonlinear problems. Numerical examples, including wave propagation in inhomogeneous media and solute transport in unsaturated porous media illustrate the proposed method.

Keywords. multiscale method, reduced basis, oscillatory PDEs

AMS subject classifications. 65N30, 74Q05, 74Q10, 74Q15

1 Introduction

The use of multiscale models throughout engineering is nowadays ubiquitous. For example, fluid flow problems in heterogeneous media, the characterization of material properties such as conductivity, deformation or crack propagations in composite materials, or chemical processes in biology all need mathematical models taking into account different physical processes at different scales. While in some applications different physical models might be used on different scales (quantum mechanics, molecular mechanics or continuum mechanics), we will focus in this contribution on physical models described by partial differential equations (PDEs) with multiple scales.

Consider therefore a family of PDEs with appropriate boundary conditions

$$L_\varepsilon(u^\varepsilon) = f \tag{1.1}$$

parametrized by ε, where $u^\varepsilon : \Omega \longrightarrow \mathbb{R}$ and Ω is an open subset of $\mathbb{R}^d$, $1 \leq d \leq 3$. The parameter ε emphasizes the multiscale nature of the above family of PDEs, and represents

[1]ANMC, Section de Mathématiques, École Polytechnique Fédérale de Lausanne, 1015 Lausanne, Switzerland, Assyr.Abdulle@epfl.ch, Yun.Bai@epfl.ch

a typical microscopic length scale of a heterogeneity in the system (oscillatory source term f^ε or multiple microscopic length scale considered by indexing the family of PDEs by $\varepsilon = (\varepsilon_1(\varepsilon), \ldots, \varepsilon_N(\varepsilon))$ could be considered as well).

Numerous numerical techniques such as the finite element method (FEM), the finite difference method (FDM) or the finite volume method (FVM) are nowadays available for the numerical discretization of (1.1). A major issue, however, is the need to resolve the finest length scale in the problem leading to a typical grid or mesh size $h < \varepsilon$. For example thermal management of multiphase composite with typical microstructures of about hundred micrometers would need a mesh of several billions points for a three-dimensional computation with a material of size $\mathcal{O}(1)$. Fortunately, appropriate averaging techniques such as the homogenization method have been developed in the past several decades [1, 2, 3, 4, 5, 6, 7] that allow for alternative numerical strategies. In these approaches, one characterizes the limit u^ε (or the limit of an appropriate flux of u^ε) as ε goes to zero and identifies an averaged equation $L_0(u^0) = f$ for the identified limit u^0. Several questions then arise such as whether the sequence u^ε converges and in which sense, whether the limit function (if it exists) solves a PDE, whether this PDE can be determined and finally whether u^0 is a good approximation of u^ε. The rigorous treatment of these questions is at the core of the mathematical homogenization theory.

The homogenization theory is also at the core of most of the numerical methods for PDEs with multiple scales. We mention for example

- methods that supplement oscillatory functions to a coarse FE space, pioneered by Babuška and Osborn [8], generalized through the so-called multiscale finite element method (MsFEM) [9], developed since then by many authors (MsFEM using harmonic coordinates [10],[11], see [12] for a survey and additional references),

- methods based on the variational multiscale method (VMM) introduced in [13] and the residual free bubble method (RFB) [14] that are closely related to MsFEM type strategy for homogenization problems [15],

- methods based on the two-scale convergence theory and its generalization [3, 16] as proposed in [17] and developed in [18] using sparse tensor product FEM,

- projection-based numerical homogenization method based on projecting a fine scale discretized problem into a low-dimensional space and eliminating successively the fine scale components [19, 20],

- numerical homogenisation methods that supplements effective data for coarse FE computation and approximate the fine scale solution via reconstruction such as the heterogeneous multiscale method (HMM) [21, 22] or related micro-macro methods [23, 24, 25, 26].

In this paper we focus on the aforementioned HMM. In the context of multiscale PDEs, this method relies on the following steps

- a macro scale method such as the finite element method (FEM), the finite difference method (FDM), or the finite volume method (FVM) defined on a macroscopic triangulation $\mathcal{T}_H$ of the physical domain $\Omega = \cup_{K\in\mathcal{T}_H} K$. The macro scale method solves an upscaled partial differential equation $L_H(u^H) = f$, where L_H is an a priori unknown approximation of L_0 recovered from microscale computations.

- constrained micro simulations defined on a microscopic triangulation $\mathcal{T}_h$ of sampling domains $K_{\delta j} = x_{Kj} + \delta Y$, where $Y = (-1/2, 1/2)^d$, $\delta \geq \varepsilon$, and $x_{Kj} \in K$ are appropriate quadrature points. The microscale method solves a problem involving the original differential operator $L_\varepsilon(\cdot)$ usually with zero forces and with boundary conditions imposed from the macro state u^H.

Our main aim is to present a reduced order modelling technique, that can be combined with numerical homogenization techniques such as the HMM, to address the complexity issue of the classical numerical homogenization methods. This method, called the reduced basis finite element heterogeneous multiscale method (RB-FE-HMM), has been introduced in [27], combined with adaptive macroscopic methods in [28] and generalized for a class of nonlinear problem in [29]. In this contribution, we want to review the RB-FE-HMM and present an unified framework for this method by explaining its use for a variety of problems, including multiscale elliptic, parabolic and wave equations and a class of non-linear elliptic or parabolic multiscale problems. In the RB-FE-HMM, a low dimensional subspace, the so-called reduced basis (RB) space is constructed in an offline stage by a greedy algorithm. The offline stage is only performed once and the outputs can be repeatedly used for many-query contexts in a co-called online stage, where the unknown effective parameters of the macroscopic solution are computed in the RB space. The moderate dimension of the RB space result in a computational cost for the online stage often comparable to a single scale FEM. As demonstrated in the numerical examples, the RB-FE-HMM presents significant efficiency advantage over the FE-HMM and can be easily combined with different model problems and macro solvers.

This paper is organized as follows. In Section 2, we introduce several model problems considered in this paper and briefly review the homogenization theory. The FE-HMM framework is reviewed in Section 3 for the various model problems and in Section 4 we present a priori error estimates and a complexity analysis for the FE-HMM. We present the RB-FE-HMM in Section 5 with a uniform description for all the model equations. The proposed reduced order modeling strategy is then tested in Section 6 at several numerical examples, including wave propagation in inhomogeneous media and solute transport in unsaturated porous media.

2 Model problem, homogenization and FE-HMM

In this section we describe various PDEs with highly oscillatory coefficients and discuss briefly the averaging procedure called homogenization.

Our physical domain will always be a bounded polyhedron Ω in $\mathbb{R}^d$ with $d \leq 3$. In order to explain our methodology we consider second-order linear elliptic equations of the form

$$\begin{aligned} -\nabla \cdot (a^\varepsilon(x) \nabla u^\varepsilon(x)) &= f(x) \quad \text{in } \Omega, \\ u^\varepsilon(x) &= 0 \quad \text{on } \partial\Omega, \end{aligned} \tag{2.2}$$

where $f \in L^2(\Omega)$. Here we choose a zero Dirichlet boundary condition for simplicity.

We will then explain how the same methodology can be applied to the following PDEs with appropriate initial and boundary conditions

- linear parabolic equations

$$\frac{\partial u^\varepsilon(x,t)}{\partial t} - \nabla \cdot (a^\varepsilon(x) \nabla u^\varepsilon(x,t)) = f(x,t) \ \text{ in } \Omega \times [0,T], \tag{2.3}$$

- linear wave equations

$$\frac{\partial^2 u^\varepsilon(x,t)}{\partial t^2} - \nabla \cdot (a^\varepsilon(x)\nabla u^\varepsilon(x,t)) = f(x,t) \ \text{ in } \Omega \times [0,T], \tag{2.4}$$

- nonlinear elliptic equations

$$-\nabla \cdot (a^\varepsilon(x,u^\varepsilon(x))\nabla u^\varepsilon(x)) = f(x) \ \text{ in } \Omega, \tag{2.5}$$

- nonlinear parabolic equations

$$\frac{\partial u^\varepsilon(x,t)}{\partial t} - \nabla \cdot (a^\varepsilon(x,u^\varepsilon(x,t))\nabla u^\varepsilon(x,t)) = f(x,t) \ \text{ in } \Omega \times [0,T]. \tag{2.6}$$

In the above equations, a^ε is a linear or nonlinear tensor that oscillates rapidly in space at the scale ε, which denotes a small scale in the problem such as the size of a typical heterogeneity under consideration in a porous medium, or the size of a typical microstructure in a composite material, etc. Solving any of the above equations by a standard FEM (or any other numerical method) requires, for small ε, a very fine meshsize $h < \varepsilon$ leading to a prohibitive computational cost.

2.1 Homogenization

In mathematical homogenization, one aims to describe an averaged equation corresponding to one of the class of PDEs with rapidly oscillating coefficients described previously. We describe briefly the homogenization procedure for the elliptic equation (2.2) and comment on similar techniques for the other equations. The formal approach based on asymptotic expansion consists in postulating an expansion $u^\varepsilon(x) = u^0(x,x/\varepsilon)+\varepsilon u^1(x,x/\varepsilon)+\varepsilon^2 u^2(x,x/\varepsilon)+\dots$ for the solution of (2.2). Here we assume that a^ε is locally periodic, i.e., $a^\varepsilon(x) = a(x,x/\varepsilon) = a(x,y)$ is y-periodic in Y (usually Y is taken as the unit cube $(-1/2,1/2)^d$) and correspondingly, we assume that the functions $u^i(x,x/\varepsilon) = u^i(x,y)$ are periodic in the second variable). Inserting the asymptotic equation in the original PDE and identifying the power of leads to an averaged (homogenized) PDE depending on an averaged tensor $a^0(x)$ that no longer depends on ε. For each macro location x, the explicit formulas of $a^0(x)$ depending on the solution of a so-called cell-problem (also referred as a micro problem in this paper) are available for locally periodic problems. The solution $u^0(x)$ of the homogenized PDE is called the homogenized solution [2]. To make this formal computation rigorous, one can use Tartar's method of oscillating test functions [30] (see also [2]) to show that $u^\varepsilon \rightharpoonup u^0$ weakly in $H_0^1(\Omega)$, $a^\varepsilon \nabla u^\varepsilon \rightharpoonup a^0 \nabla u^0$ weakly in $(L^2(\Omega))^d$.

Departing from the locally periodic case, there exists more general theory such as the $H-$convergence [30]. As a starting point, we have to consider a family of equations, corresponding to a family of tensors tensors a^ε indexed by ε, that are uniformly elliptic and bounded, i.e., there exist positive $\lambda, \Lambda \in \mathbb{R}$ such that for any $\xi \in \mathbb{R}^d$

$$\lambda|\xi|^2 \le a^\varepsilon(x)\xi \cdot \xi, \quad |a^\varepsilon(x)\xi| \le \Lambda|\xi|, \qquad \text{a.e. } x \in \Omega, \forall\, \varepsilon > 0. \tag{2.7}$$

The $H-$convergence ensures then the existence of a subsequence of the matrices a^ε and a homogenized tensor a^0 (again uniformly elliptic and bounded) such that for the corresponding subsequence, u^ε and $a^\varepsilon \nabla u^\varepsilon$ converge weakly to u^0 in $H_0^1(\Omega)$ and weakly to $a^0 \nabla u^0$ in

$(L^2(\Omega))^d$, respectively. For non-periodic oscillating tensors, the homogenized tensors $a^0(x)$ are in general not known in an explicit form. Similar averaging procedure exist for the multiscale problem (2.3)-(2.6), see [2, 5, 31, 32]. For a practical solution, one has to rely on numerical approximation. The numerical methods that we describe below do not rely on a periodic tensors. The scale separation seems required for our numerical strategy to make sense. However the case of locally periodic tensors will sometimes be considered to derive a complete numerical analysis for the proposed multiscale method. Already in this situation, the determination of the homogenized tensor $a^0(x)$ depends on the macro location $x \in \Omega$ and we thus have an infinite number of cell problems to solve to obtain $a^0(x)$ and a proper approximation of $a^0(x)$ is required.

3 Numerical homogenization, micro-macro methods

We now present a numerical homogenization method, called the finite element heterogeneous multiscale method (FE-HMM) [33, 34], that is able to compute an approximation of the homogenized solution $u^0(x)$, relying on a finite number of cell problems chosen in such a way that the overall computation is efficient and reliable. In a second step, an approximation of the fine scale solution u^ε can be obtained by a reconstruction procedure.

3.1 Main ingredients

Assume for simplicity, that Ω is a polyhedral domain in $\mathbb{R}^d$, $d \leq 3$ and consider a shape-regular family of partitions $\{\mathcal{T}_H\}$ of Ω in simplicial or quadrilateral elements $K \in \mathcal{T}_H$ of diameter H_K where we denote $H := \max_{K\in\mathcal{T}_H} H_K$. As H is not required to be smaller or even commensurate to ε, we call this triangulation a macroscopic triangulation of Ω. In its simplest form the FE-HMM relies on the following ingredients

1. a macroscopic FE method based on a macroscopic triangulation of Ω,
2. a quadrature formula on each macroscopic element K of the macroscopic triangulation,
3. microscopic FE methods defined on sampling domains around the integration points in K used to recover the effective parameters (e.g., macroscopic conductivity) around the integration points.

We next describe the different ingredients listed above. A commonly used macroscopic FE space is given by

$$V_H(\Omega) = \{v^H \text{ is continuous on } \Omega,\ v^H = 0 \text{ on } \partial\Omega;\ v^H|_K \in \mathcal{R}^\ell(K),\ \forall K \in \mathcal{T}_H\},$$

where $\mathcal{R}^\ell(K)$ is the space $\mathcal{P}^\ell(K)$ of polynomials on K of total degree at most ℓ if K is a simplicial FE, or the space $\mathcal{Q}^\ell(K)$ of polynomials on K of degree at most ℓ in each variable if K is a quadrilateral FE. We note that for some problems for which mass conservation is required, other macroscopic FE space should be used. We mention for example the discontinuous Galerkin FE-HMM proposed and analyzed for elliptic problem in [35] and for advection-diffusion problem (with possible high Peclet number) in [36].

For each element K of the macro partition we consider a quadrature formula $(\omega_{K_j}, x_{K_j})_{j=1,\dots,J}$ with weights ω_{K_j} and nodes x_{K_j} fulfilling classical assumptions (see Section 4 and [37]).

Finally the microscopic FE method is defined as follows. Define for each quadrature node x_{K_j} a sampling domain $K_{\delta_j} = x_{K_j} + \delta Y$. On this sampling domain we consider a simplicial micro mesh $\mathcal{T}_h$ and the micro finite element space $V_h(K_{\delta_j})$ defined by

$$V_h(K_{\delta_j}) = \{z^h \in W(K_{\delta_j}) \,|\, z^h|_T \in \mathcal{R}^q(T), \forall\, T \in \mathcal{T}_h\}, \tag{3.8}$$

where the choice of $W(K_{\delta_j})$ determines the boundary conditions used for computing the micro functions $v^h_{K_j}$. We consider two different spaces:

- periodic coupling: $W(K_\delta) = W^1_{per}(K_\delta) = \left\{v \in H^1_{per}(K_\delta) \,|\, \int_{K_\delta} v\, dx = 0\right\}$;
- Dirichlet coupling: $W(K_\delta) = H^1_0(K_\delta)$.

The micro problems depend on the specific problem (2.2)-(2.6). For (2.2), given a macroscopic function $v^H \in V_H(\Omega)$, we consider the linearization $v^H_{lin,j}(x) := v^H(x_{K_j}) + (x - x_{K_j}) \cdot \nabla v^H(x_{K_j})$ and the following problem: find $v^h_{K_j}$ such that $v^h_{K_j} - v^H_{lin,j}(x) \in V_h(K_{\delta_j})$ and

$$\int_{K_{\delta_j}} a^\varepsilon(x) \nabla v^h_{K_j}(x) \cdot \nabla z^h(x) dx = 0 \quad \forall z^h \in V_h(K_{\delta_j}). \tag{3.9}$$

3.2 The FE-HMM for linear problem

At the macroscopic level, the numerical method is defined as follows: find $u^H \in V_H(\Omega)$ such that

$$B_H(u^H, v^H) = \int_\Omega f v^H dx \quad \forall v^H \in V_H(\Omega), \tag{3.10}$$

where

$$B_H(v^H, w^H) := \sum_{K \in \mathcal{T}_H} \sum_{j=1}^{J} \frac{\omega_{K_j}}{|K_{\delta_j}|} \int_{K_{\delta_j}} a^\varepsilon(x) \nabla v^h_{K_j}(x) \cdot \nabla w^h_{K_j}(x) dx. \tag{3.11}$$

In (3.11) $v^h_{K_j}$ (respectively $w^h_{K_j}$) denotes the solution of the micro problem (3.9). The following reformulation of the above macro problem is useful for the analysis of the method, namely

$$B_H(v^H, w^H) = \sum_{K \in \mathcal{T}_H} \sum_{j=1}^{J} \omega_{K_j} a^{0,h}(x_{K_j}) \nabla v^H(x_{K_j}) \cdot \nabla w^H(x_{K_j}), \tag{3.12}$$

where

$$\left(a^{0,h}(x_{K_j})\right)_{mn} = \frac{1}{|K_{\delta_j}|} \int_{K_{\delta_j}} a^\varepsilon(x)(\nabla \psi^h_\tau(x) + \mathbf{e}_m) \cdot \mathbf{e}_n dx, \tag{3.13}$$

with $\tau = (x_{K_j}, m)$ and $\psi^h_\tau \in V_h(K_{\delta_j})$ and $\psi^h_\tau + x_m$ is the solution of (3.9) that can be rewritten as

$$\int_{K_{\delta_j}} a^\varepsilon(x) \nabla \psi^h_\tau(x) \cdot \nabla z^h(x) dx = -\int_{K_{\delta_j}} a^\varepsilon(x) \mathbf{e}_m \cdot \nabla z^h(x) dx \quad \forall z^h \in V_h(K_{\delta_j}) \tag{3.14}$$

where $\mathbf{e}_m$, $m = 1, \ldots, d$ denotes the canonical basis of $\mathbb{R}^d$. For a proof of this equivalence we note that $v^h_{K_j} - v^H_{lin,j}(x)$ can be represented by a linear combination of $\psi^h_\tau(x)$, $\tau =$

(x_{K_j}, m), $m = 1, \ldots, d$ (see [38] for details). We next explain how the FE-HMM can be generalized for parabolic, wave and nonlinear equations. We only focus on the reformulation of the form (3.12). We close this section by noting that for practical computation $f(x)$ should be replaced by an appropriate approximation $f_H(v^H)$ in a finite element space. Here and in what follows we will work with exact right-hand side for simplicity. The FE-HMM for parabolic homogenization problem (2.3) reads: find $u^H(t) : [0, T] \to V_H(\Omega)$, such that

$$(\partial_t u^H(t), v^H) + B_H(u^H(t), v^H) = \int_\Omega f v^H dx \quad \forall v^H \in V_H(\Omega), \tag{3.15}$$

while for the wave equation it reads: find $u^H(t) : [0, T] \to V_H(\Omega)$ such that

$$(\partial_{tt} u^H(t), v^H) + B_H(u^H(t), v^H) = \int_\Omega f v^H dx \quad \forall v^H \in V_H(\Omega), \tag{3.16}$$

where the bilinear form $B_H(\cdot, \cdot)$ is defined by (3.12) for both problems and initial and boundary conditions must be supplemented.

3.3 The FE-HMM for nonlinear problems

We start with the nonlinear homogenization problem (2.5). The FE-HMM reads: find $u^H \in V_H(\Omega)$ such that

$$B_H(u^H; u^H, w^H) = \int_\Omega f v^H dx = F(w^H), \quad \forall w^H \in V_H(\Omega), \tag{3.17}$$

where

$$B_H(z^H; v^H, w^H) := \sum_{K \in \mathcal{T}_H} \sum_{j=1}^{J} \omega_{K_j} a^{0,h}\big(x_{K_j}, z^H(x_{K_j})\big) \nabla v^H(x_{K_j}) \cdot \nabla w^H(x_{K_j}). \tag{3.18}$$

The component of the tensor $a^{0,h}\big(x_{K_j}, s\big)$ are defined as in (3.13) using (3.14), where in both equations $a^\varepsilon(x)$ must be replaced by $a^\varepsilon(x, s)$. The parameter τ for $\psi_\tau^h(x)$ now depends on $\tau = (x_{K_j}, s, m)$.

Using Newton iterations for the nonlinear problem (3.17), we consider a sequence $u_k^H, k = 0, 1, 2, 3, \ldots$ satisfying the following iteration scheme,

$$\partial B_H(u_k^H; u_{k+1}^H - u_k^H, w^H) = F(w^H) - B_H(u_k^H; u_k^H, w^H), \quad \forall w^H \in V_H(\Omega), \tag{3.19}$$

where $\partial B_H(z^H; v^H, w^H) := B_H(z^H; v^H, w^H) + B'_H(z^H; v^H, w^H)$, and

$$B'_H(z^H; v^H, w^H) := \sum_{K \in \mathcal{T}_H} \sum_{j=1}^{J} \omega_{K_j} \partial_s a^{0,h}\big(x_{K_j}, z^H(x_{K_j})\big) v^H(x_{K_j}) \nabla z^H(x_{K_j}) \cdot \nabla w^H(x_{K_j}),$$

where $\partial_s a^{0,h}$ denotes the derivative of $a^{0,h}$ with respect to the second variable.

Finally for nonlinear parabolic problems of the type (2.6) the FE-HMM read: find $u^H(t) : [0, T] \to V_H(\Omega)$, such that

$$(\partial_t u^H(t), v^H) + B_H(u^H(t); u^H(t), w^H) = F(w^H) \quad \forall w^H \in V_H(\Omega). \tag{3.20}$$

4 A priori estimates, fine scale reconstruction and complexity

In this section we discuss a priori error estimates for the various FE-HMM methods introduced above. First, we observe that appropriate conditions on the quadrature formula are needed to ensure well-posedness of the macro problem and optimal convergence. The following assumptions are the usual requirement for single scale FEM with numerical quadrature (see [37]). We consider nodes and weights $\{\hat{x}_j, \hat{\omega}_j\}_{j=1}^J$ on the reference element $\hat{K}$ (the corresponding nodes and weights on element $K \in \mathcal{T}_H$ are then obtained using a C^1- diffeomorphism from $\hat{K}$ to K)

(**Q1**) $\hat{\omega}_j > 0,\ j = 1, \ldots, J, \quad \sum_{j=1}^J \hat{\omega}_j |\nabla \hat{p}(\hat{x}_j)|^2 \geq \hat{\lambda} \|\nabla \hat{p}\|^2_{L^2(\hat{K})},\ \forall \hat{p}(\hat{x}) \in \mathcal{R}^\ell(\hat{K}),\ \hat{\lambda} > 0;$

(**Q2**) $\int_{\hat{K}} \hat{p}(\hat{x}) d\hat{x} = \sum_{j=1}^J \hat{\omega}_j \hat{p}(\hat{x}_j),\ \forall \hat{p}(\hat{x}) \in \mathcal{R}^\sigma(\hat{K})$, where $\sigma = \max(2\ell - 2, \ell)$ if $\hat{K}$ is a simplicial FE, or $\sigma = \max(2\ell - 1, \ell + 1)$ if $\hat{K}$ is a rectangular FE.

4.1 A priori estimates

The general methodology to estimate the error between the FE-HMM solution u^H and the homogenized solution u^0 of any of the problems (2.2)-(2.6) is based on a decomposition in macro, modeling and micro errors as described below (see also [39]). We first introduce two auxiliary FE functions, namely $u^{0,H}$, the solution of any of the homogenized problems obtained by a FEM with numerical quadrature, and $\bar{u}^H$ the FE-HMM solution of any of the problems (2.2)-(2.6), but with a form $\bar{B}_H$ obtained with exact micro functions. Both $u^{0,H}$ and $\bar{u}^H$ are only introduced to analyze the various contribution to the error and we emphasize that these solutions cannot be obtained in practical applications. Indeed to obtain $u^{0,H}$ one needs to know the exact homogenized tensor that is not available in general and to obtain $\bar{u}^H$ one needs to know the exact solution of the micro problems. We then consider the following decomposition

$$\|u^0 - u^H\| \leq \underbrace{\|u^0 - u^{0,H}\|}_{e_{mac}} + \underbrace{\|u^{0,H} - \bar{u}^H\|}_{e_{mod}} + \underbrace{\|\bar{u}^H - u^H\|}_{e_{mic}}, \tag{4.21}$$

where $\|\cdot\|$ stands for the L^2 or H^1 norms for elliptic problems, the $L^2([0,T]; H^1(\Omega))$ or $L^\infty([0,T]; L^2(\Omega))$ norms for parabolic problems, and the $L^\infty([0,T]; H^1(\Omega))$ or $L^\infty([0,T]; L^2(\Omega))$ norms for the wave problem. Of course, the rigorous analysis will depend on the type of problem under consideration, but one common feature is that variational crimes are committed in the FE-HMM in the sense that the exact homogenized form $B_0(\cdot,\cdot)$ differs from its numerical counterpart $B_H(\cdot,\cdot)$ and hence standard Galerkin orthogonality arguments fail. This complicates the analysis specially for nonlinear problems [40, 41], non conforming FE discretization [35, 36] or time-dependent problems [42, 43].

Another common issue is that the micro errors are transmitted to the macro scale resulting in an error in the effective data. The so-called fully discrete analysis, first given in [33] for the FE-HMM, gives an indication of the complexity of the numerical method and indicates how to balance micro and macro mesh sizes in order to achieve a given accuracy with a minimal computational cost.

Finally, the modeling error encodes the geometric error due to the mismatch between macro computational domain size and the size of the micro period and the error done in imposing (artificial) boundary conditions in the micro sampling domains (determined by the choice of the micro FE space (3.8) that sets the coupling conditions between micro and

macro FE functions). To be more specific, we mention the a priori error estimates for elliptic problems obtained in [33, 39, 34].

Theorem 4.1 *Let u^0 be the homogenized solution corresponding to the problem* (2.2) *and u^H be the solution of problem* (3.10)*. Assume that* (2.7)*, (***Q1***), and (***Q2***) hold. Then, under sufficient regularities of the tensor a^ε and the right-hand side f, we have the following estimates*

$$\|u^0 - u^H\|_{H^1(\Omega)} \leq C\left(H^l + \left(\frac{h}{\varepsilon}\right)^{2q} + e_{mod}\right), \tag{4.22}$$

$$\|u^0 - u^H\|_{L^2(\Omega)} \leq C\left(H^{l+1} + \left(\frac{h}{\varepsilon}\right)^{2q} + e_{mod}\right), \tag{4.23}$$

where C is independent of H, h and ε.

The modeling error does not depend on the micro or macro mesh size. For locally periodic coefficients it is possible to show that $e_{mod} = 0$ using a slightly modified FE-HMM (collocated version) when $\delta/\varepsilon \in \mathbb{N}$ and for the micro FE space subset of $W^1_{per}(K_\delta)$. When $\delta/\varepsilon \notin \mathbb{N}$ and $W(K_\delta) = H^1_0(K_\delta)$, one can show that $e_{mod} \leq C\left(\frac{\varepsilon}{\delta} + \delta\right)$ [34].

A priori error estimates similar to Theorem 4.1 have been obtained for parabolic problems of the type (2.3) in [43], for nonlinear elliptic problems of the type (2.5) in [40, 41] and for wave problems of type (2.4) in [42].

4.2 Fine scale reconstruction

While the numerical methods described in Sections 3.2 and 3.3 allow to compute an approximation u^H of the homogenized solution u^0, they do not allow to approximate the fine scale solution u^ε of (2.2)-(2.6) in the energy norms. We note however that in the L^2 norm u^H is still a good approximation of u^ε due to the error estimate $\|u^\varepsilon - u^0\| \leq C\varepsilon$ that holds for sufficiently regular problems [5].

Using the FE-HMM, we can nevertheless recover a fine scale approximation of u^ε following a post-processing procedure inspired by [44]. Let $D \subset \Omega$ be the region of the computational domain where we want to approximate u^ε and assume that u^H has been computed on Ω.

We start by explaining the reconstruction procedure for the linear problem 2.2. Define then $D \subset D_\eta \subset \Omega$, where $\text{dist}(\partial D, \partial D_\eta) = \eta$ and consider the following problem: find $u^{Hh} - u^H \in \mathcal{V}_h(D_\eta) \subset H^1_0(D_\eta)$ such that

$$\int_{D_\eta} a^\varepsilon(x)\nabla u^{Hh} \cdot \nabla z^h dx = 0 \quad \forall z^h \in V_h(D_\eta).$$

The following error estimate is valid under appropriate regularity assumptions [34]

$$\int_D |\nabla(u^\varepsilon - u^{Hh})|^2 dx \leq \frac{C}{\eta}\left(\|u^0 - u^H\|_{L^\infty(D_\eta)} + \|u^\varepsilon - u^0\|_{L^\infty(D_\eta)}\right).$$

For locally periodic homogenization problem a simpler and cheaper reconstruction can be obtained. Indeed, consider for example the FE-HMM with piecewise linear macro FE functions and the micro functions $u^h - u^H$ available in each K_δ (observe that for piecewise linear

macro FEM, there is only one sampling domain per macro element). Next extend these micro functions periodically in K (we denote this extension by $u_{h,K}$) and consider the reconstruction

$$u^{Hh}(x) = u^H(x) + u^{h,K}(X),\ x \in K,\ \forall K \in \mathcal{T}_H. \tag{4.24}$$

Assuming that $V_h(K_\delta) \subset W^1_{per}(K_\delta)$ and $\delta/\varepsilon \in \mathbb{N}$ then the following error estimate hold [33, 34]

$$\|u^\varepsilon - u^{Hh}\|_{\bar{H}^1(\Omega)} \leq C\left(H + \frac{h}{\varepsilon} + \sqrt{\varepsilon}\right),$$

where C is independent of H, h, ε and $\|u\|_{\bar{H}^1(\Omega)} = \left(\sum_{K\in\mathcal{T}_H} \|\nabla u\|^2_{L^2(K)}\right)^{1/2}$ denotes a broken semi-norm. This result is based on a corrector results for homogenization problems, i.e., a function $u^{1,\varepsilon}$ such that $u^\varepsilon \simeq u^0 + u^{1,\varepsilon}$. For locally periodic problems, such functions $u^{1,\varepsilon}$ is obtained from the solution of localized micro problems of the type (3.9) (in a periodic Sobolev space) and the convergence results $\|u^\varepsilon - (u^0 + u^{1,\varepsilon})\|_{H^1(\Omega)} \leq C\sqrt{\varepsilon}$ holds for smooth problems [5].

For the nonlinear problem (2.5) a similar procedure can be employed [40, 41] thanks to the results in [45, Sect. 3.4.2]. There it is shown that any corrector $u^{1,\varepsilon}$ for the linear problem obtained from (2.5) by replacing $a^\varepsilon(x, u^\varepsilon(x))$ with $a^\varepsilon(x, u^0(x))$, where u^0 is the solution of the corresponding homogenization problem, is is also a corrector for the solution u_ε of the nonlinear problem (2.5) and that

$$\nabla r_\varepsilon \to 0 \text{ strongly in } (L^1_{loc}(\Omega))^d \text{ where } r_\varepsilon(x) := u^\varepsilon(x) - u^0(x) - u^{1,\varepsilon}(x). \tag{4.25}$$

Hence, a similar reconstruction as defined in (4.24) can be used and for locally periodic problems assuming again $V_h(K_\delta) \subset W^1_{per}(K_\delta)$ and $\delta/\varepsilon \in \mathbb{N}$ we have

$$\|u^\varepsilon - u^{Hh}\|_{\bar{H}^1(\Omega)} \leq C(H + h/\varepsilon + \varepsilon) + \|r_\varepsilon\|_{\bar{H}^1(\Omega)},$$

where C is independent of H, h, ε and r_ε is defined in (4.25).

4.3 Complexity

The convergence rates in Theorem 4.1 show a classical rate for the macro error and a better than usual rate in the micro error (loosely speaking this is due to the fact the product of micro functions enter in the bilinear form $B_H(\cdot,\cdot)$, see [33, 46, 41] for details).

We next discuss the computational cost of the FE-HMM. If we denote N_{mic} the number of degrees of freedom (DOF) in each space dimension for the discretization of the sampling domain K_{δ_j}, we obtain $h = \delta/N_{mic}$ hence $\hat{h} = (\delta/\varepsilon)\cdot(1/N_{mic})$. By noting that δ scales with ε (e.g., $\delta = C\varepsilon$ with C a constant of moderate size) we have $\hat{h} = (C/N_{mic})$. We next denote by $M_{mic} = \mathcal{O}(\hat{h}^{-d})$ the number of DOF for the micro FEM and by M_{mac}, the number of DOF of the macro FEM. The macro meshsize H and the micro meshsize $\hat{h}$ are related to M_{mac} and M_{mic} (for quasi-uniform macro meshes) as

$$H = \mathcal{O}(M_{mac}^{-1/d}), \qquad \hat{h} = \mathcal{O}(M_{mic}^{-1/d}).$$

and according to the a priori error estimates of Theorem 4.1 optimal macroscopic convergence rates require

$$\hat{h} \simeq H^{\frac{\ell}{2q}} \quad \text{for the } H^1 \text{ norm}, \quad \hat{h} \simeq H^{\frac{\ell+1}{2q}} \quad \text{for the } L^2 \text{ norm}.$$

with an induced complexity given by

$$\underbrace{H^{-d}}_{M_{mac}} \cdot \underbrace{H^{\frac{-d\ell}{2q}}}_{M_{mic}} \cdot n_s = (M_{mac})^{1+\frac{\ell}{2q}} \cdot n_s \qquad \text{for the } H^1 \text{ norm,}$$

$$\underbrace{H^{-d}}_{M_{mac}} \cdot \underbrace{H^{\frac{-d(\ell+1)}{2q}}}_{M_{mic}} \cdot n_s = (M_{mac})^{1+\frac{\ell+1}{2q}} \cdot n_s \qquad \text{for the } L^2 \text{ norm,}$$

where n_s denotes the number of sampling domains per macro element $K \in \mathcal{T}_H$.

We first notice that the method is *independent* of the size of the oscillatory parameter ε. This is in sharp contrast with classical FEMs that would require a computational cost that scales with ε as $\mathcal{O}(\varepsilon^{-d})$. Second, it can be seen, as first noticed in [33], that the complexity is superlinear with respect to the macro DOF. As an example, if we choose piecewise linear simplicial FEs and assume that the complexity is proportional to the total DOF we obtain a cost of $\mathcal{O}(M_{mac}^{3/2})$ (H^1 norm) and $\mathcal{O}(M_{mac}^2)$ (L^2 norm).

Of course the method is well suited for parallel implementation as the micro problems are solved independently. We also note that the memory requirement is proportional to $M_{mac} + M_{mic}$ only as the micro problem, being independent of one another, can be solved one at a time. Finally, as investigated in [47], using spectral method or *p-FEM* for the micro solvers can reduce the complexity of the FE-HMM down to a log-linear complexity. This approach however requires high regularity of the oscillating tensor a^ε. Another tools allowing for a reduction of the computational cost is the use of adaptive techniques at the macro scale. Indeed, micro computations can be recycled in macro elements that are not refined, see [48].

5 Reduced order modeling numerical homogenization

The key issue that leads to a superlinear computational cost in a numerical homogenization method such as the FE-HMM is the need of repeated computation of micro problems (3.14) at each quadrature point. At the same time in view of Theorem 4.1, an increasing number of micro DOF as the macroscopic mesh gets refined is needed. This issue has triggered the development of a reduced order modeling strategy for the FE-HMM. The framework is built on the so-called reduced basis methodology [49, 50, 51] first used in the context of numerical homogenization in [52, 53] and for the FE-HMM in [27, 28, 29]. The new method is called the reduced basis finite element heterogeneous multiscale method (RB-FE-HMM).

The main observation is the following: instead of computing micro problems in each macro elements at the quadrature points, we identify in *an offline stage* a small number N of precomputed representative micro solutions to construct a reduced basis (RB) space. The selected parameters τ which determine those representative micro solutions are selected by greedy algorithm based on a large parameter training set (see Figure 1). A key tool in the greedy algorithm is the use of a posteriori error estimator to select the parameter τ for which the micro solutions vary the most.

The actual macro computation is done in an online stage, and the missing effective data are computed at the required quadrature points of the macro elements $K \in \mathcal{T}_H$ by solving the micro problem in the pre-computed RB space (of dimension N) which leads to solving small linear systems of size $N \times N$.

We see that for the RB-FE-HMM, the repeated micro FEM computation and micro mesh refinement are avoided though the pre-computation of a fixed low dimensional approximation space (the RB space). In addition, the RB space is independent of the macro solvers which

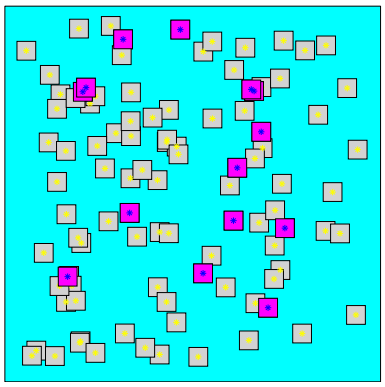

Fig. 1: Selection of sampling domains in the offline stage (pink color) where micro problems are computed, among a random collection of sampling domains (training set).

can be repeatedly used with different macroscopic partitions and different types of problems (static or evolutionary). In what follows, we give some details of both the online and the offline stages.

5.1 Offline stage

We observe that the solutions of the micro problems for any of the problems (3.10), (3.16), (3.17) or (3.20), depend on the parameter $\tau = (x, m)$ (linear problems) or $\tau = (x, m, s)$ (nonlinear problem). To treat both cases at the same time, we will set $\tau = (\kappa, m)$, where $\kappa = x$ (linear case) and $\kappa = (x, s)$ (nonlinear case). The fundamental condition for the efficiency of the RB method is that the multiscale tensor $a^\varepsilon(x, s)$ has an affine representation. We first set a correspondence of an arbitrary sampling domain included in Ω namely $K_\delta = x + \delta y$ with $y \in Y = (-1/2, 1/2)^d$ through the affine transformation

$$y \in Y \mapsto G_x(y) = x + \delta y \in K_\delta. \tag{5.26}$$

We can then map the tensors $a^\varepsilon(x)$ or $a^\varepsilon(x, s)$ into the reference domain $Y = (-1/2, 1/2)^d$

$$a_x(y) := a^\varepsilon(G_x(y)) \text{ (linear case)}, \quad a_{x,s}(y) := a^\varepsilon(G_x(y), s) \text{ (nonlinear case)}. \tag{5.27}$$

When it yields no confusion we will simply write $a_\kappa(y)$ for either situation. A crucial assumption for the RB methodology is that $a_\kappa(y)$ has an affine representation of the form

$$a_\kappa(y) = \sum_{p=1}^{P} \Theta_p(\kappa) a_p(y), \ \forall y \in Y. \tag{5.28}$$

For example, for a tensor of the form $a^\varepsilon(x) = a(x, x/\varepsilon) = (\alpha + x \sin(x/\varepsilon))I$, where I is the $d \times d$ identity matrix and α a scalar, the above representation exists. When such an explicit representation is not available, one can use a greedy algorithm, called the empirical interpolation method (EIM), to approximate a nonaffine tensor by an affine one of the form (5.28) (see [54]).

We next map the micro problem (3.14) (or its nonlinear version) for an arbitrary sampling domain $K_\delta = x + \delta y$ included in Ω to the reference domain Y by using the change of variable

$G_x(y)$

$$\int_Y a_\kappa(y)\nabla\hat{\psi}^h_\tau(y)\cdot\nabla\hat{z}^h(y)dy = -\int_Y a_\kappa(y)\mathbf{e}_m\cdot\nabla\hat{z}^h(y)dy \quad \forall\hat{z}^h\in V_h(Y), \tag{5.29}$$

where $\tau=(\kappa,m)$ and $\psi^h_\tau(G_x(y))=\delta\hat{\psi}^h_\tau(y)$.

We next choose a set of parameter $\mathcal{D}\times\{1,\dots,d\}$, where $\mathcal{D}$ is a compact subspace of Ω for linear problems and a compact subspace of $\Omega\times\mathbb{R}$ for nonlinear problems. The construction of the RB space is done in an offline procedure, where a small number $\{\tau_1,\dots,\tau_N\}$ of representative micro problems with $\tau_i=(\kappa_i,m_i)\in\mathcal{D}\times\{1,\dots,d\}$ are selected by a Greedy algorithm. The corresponding FE solutions $\hat{\psi}^h_{\tau_i}(y)$ of the cell problem (5.29) for these selected parameters will give the reduced basis functions $\hat{\xi}_i$ obtained from $\hat{\psi}^h_{\tau_1},\dots,\hat{\psi}^h_{\tau_N}$ through normalization and orthogonalization. Hence, we obtain the reduced basis space $S_N:=\{\hat{\xi}_1,\dots,\hat{\xi}_N\}$.

Algorithm 5.1 *(Offline procedure) Define a training set Ξ_{RB}, an offline tolerance tol_{RB}, and compute for a random selected $\tau_1\in\Xi_{RB}$ the fist RB function $\hat{\xi}_1=$ $frac\hat{\psi}^h_{\tau_1}\|\hat{\psi}^h_{\tau_1}\|$,*

1. *assume that $S_\ell:=\{\hat{\xi}_1,\dots,\hat{\xi}_\ell\}$ is computed, compute $\hat{e}_{RB}(\tau):=\nabla(\hat{\psi}^h_\tau-\hat{\psi}^\ell_\tau),\ \forall\tau\in\Xi_{RB}$, where $\hat{\psi}^\ell_\tau$ is the micro solution solved in S_ℓ;*

2. *if $\max_{\tau\in\Xi_{RB}}\|\hat{e}_{RB}(\tau)\|_{L^2(Y)}<tol_{RB}$, the offline stage ends (appropriate data must then be stored, see (5.31) and (5.33)); otherwise, continue with the next step;*

3. *select the next representative parameter $\tau_{\ell+1}=argmax_{\tau\in\Xi_{RB}}\|\hat{e}_{RB}(\tau)\|_{L^2(Y)}$, and compute the new basis function $\hat{\xi}_{\ell+1}$. Let $\ell=\ell+1$ and go back to Step (i).*

The offline procedure is only operated once and the outputs can be repeatedly used for the later online computation. Therefore, we require the micro FEM used in the offline stage to be very accurate so that the corresponding micro FE error e_{mic} does not affect the online results.

We notice that the direct computation of $\hat{e}_{RB}(\tau)$ in Algorithm 5.1 can become quite expensive due to the computation of highly resolved micro FE solution over a large training set. This issue can be resolved by estimating $\|\hat{e}_{RB}(\tau)\|_{L^2(Y)}$ by an a posteriori error estimator Δ_τ which can be computed by solving a few pseudo-FE solutions. The a posteriori estimator for linear problems Δ^l_τ is designed in [27]. For nonlinear problem, some care is needed to construct such estimators Δ^{nl}_τ which have been derived in [29] in a numerical homogenization context. The following results have been obtained

$$\|\hat{e}_{RB}(\tau)\|_{L^2(Y)}\le C\Delta^l_\tau,\ \text{(linear problems)},$$
$$\left(\|\hat{e}_{RB}(\tau)\|^2_{L^2(Y)}+\|\partial_s\hat{e}_{RB}(\tau)\|^2_{L^2(Y)}\right)^{1/2}\le C\Delta^{nl}_\tau,\ \text{(nonlinear problems)}.$$

We also emphasize that the a posteriori error can be used in the online stage to certify the accuracy of the online solution. Appropriate procedure to compute the constant C are available. For nonlinear problem, Newton iteration is applied and we thus need to have control on the derivative of $\hat{e}_{RB}(\tau)$ with respect to the parameter s. A general result proved in [55, 56] shows that if the best N-dimensional approximation of a subset of a Hilbert space has a rapidly decaying projection error (e.g. exponential decay), then the N-dimensional space obtained from the RB method enjoys the same projection error.

5.2 Online stage

Compared to the FE-HMM, the advantage of the RB-FE-HMM is that in the online stage, all the micro problems are solved in the same RB space S_N with dimension N (usually of moderate size). Thus the computational cost for the online stage is $\mathcal{O}(M_{mac})$ and scales *linearly* with the macroscopic DOF (assuming that the cost is proportional to the total DOF).

We next detail the online procedure. To obtain the numerical homogenized solution, we still need to solve the macro problem either in form of (3.10) or (3.17). Now the unknown homogenized tensor $a^0(\kappa)$ can be estimated by

$$\big(a_N^0(\kappa)\big)_{mn} = \int_Y a_\kappa(y)\left(\nabla\hat{\psi}_\tau^N(y) + \mathbf{e}_m\right)\cdot\mathbf{e}_n dy. \tag{5.30}$$

where $\hat{\psi}_\tau^N \in S_N$. By expending $\hat{\psi}_\tau^N = \sum_{i=1}^N \beta_{i,\tau}\hat{\xi}_i$ and using the affine representation (5.28) we can further write (5.30) into

$$\big(a_N^0(\kappa)\big)_{mn} = \sum_{p=1}^P \Theta_p(\kappa)\big(\boldsymbol{\beta}_\tau F_{p,n} + (G_p)_{mn}\big), \quad m,n = 1,\dots,d,$$

where $\boldsymbol{\beta}_\tau := \big(\beta_{1,\tau},\dots,\beta_{N,\tau}\big)$. The matrices $F_{p,n}$ and G_p are the offline outputs defined as

$$(F_{p,n})_i = \int_Y a_p(y)\mathbf{e}_n\cdot\nabla\hat{\xi}_i(y)dy,\ i = 1,\dots,N, \quad (G_p)_{mn} = \int_Y (a_p(y))_{mn}dy, \tag{5.31}$$

for $m,n = 1,\dots,d$.

In order to get the coefficients $\boldsymbol{\beta}_\tau$, we need to solve the following cell problem:

$$\int_Y a_\kappa(y)\nabla\hat{\psi}_\tau^N(y)\cdot\nabla z_N(y)dy = -\int_Y a_\kappa(y)\mathbf{e}_m\cdot\nabla z_N(y)dy,\ \forall z_N\in S_N. \tag{5.32}$$

Using (5.31), (5.28) and the following offline output matrices for $p = 1,\dots,P$,

$$(A_p)_{ij} = \int_Y a_p(y)\nabla\hat{\xi}_i(y)\cdot\nabla\hat{\xi}_j(y)dy,\ i,j = 1,\dots,N, \tag{5.33}$$

equation (5.32) can be written as an $N\times N$ linear system

$$\left(\sum_{p=1}^P \Theta_p(\kappa)A_p\right)\boldsymbol{\beta}_\tau^T = -\sum_{p=1}^P \Theta_p(\kappa)F_{p,m}. \tag{5.34}$$

We note that the necessary data that needs to be stored at the end of the offline stage are only a few $N\times N$ matrices with low storage requirement. The linear system (5.34) is independent of the macro partition or the macro solvers. Furthermore for linear multiscale problems (5.34), it is independent of the right hand side function f in the multiscale model equations nor does it depend on the boundary and initial conditions for time dependent problems. Therefore, the offline outputs can be used for various macroscale scenarios.

In comparison, the micro cell problems for the FE-HMM (3.14) are solved by the micro FEM with the number of DOF $M_{mic}\approx M_{mac}$. This triggers simultaneous micro and macro refinement and leads to a significant computational overhead compared to the RB-FE-HMM.

We will study this significant difference in the performance of the FE-HMM versus RB-FE-HMM in the numerical example of Section 6.

Finally, we end this section by mentioning that the a priori error estimate of the RB-FE-HMM is similar to the FE-HMM but with one more error term arising from the RB model reduction, i.e.

$$\|u^{H,RB} - u^0\| \leq e_{mac} + e_{mic} + e_{mod} + e_{RB},$$

where $u^{H,RB}$ is the solution of (3.10) or (3.17) based on the RB-FE-HMM. Compared to the FE-HMM, the errors e_{mac} and e_{mod} remain the same, but e_{mic} is much smaller due to the offline requirement that the representative micro problems are computed accurately. The term e_{RB} is bounded by the a posteriori estimator and therefore controlled by the given offline tolerance. This a posteriori error estimator can also be computed in the online stage to certify the accuracy of the computed macro solution by quantifying the reduced basis error. A priori estimate for e_{RB} relies on appropriate assumption on best N-dimensional subspace that minimizes the projection error of an arbitrary functions in the space of solutions of cell problems, see [27, 29]. In practical computations, the RB-FE-HMM and the FE-HMM have nearly the same accuracy, provided *simultaneous refinement* of macro and micro meshes is implemented for the FE-HMM. In contrast, the computational cost for the online stage of the RB-FE-HMM is comparable to the cost of a FEM for single-scale problems and yields a substantial saving when compared to numerical homogenization methods such as the FE-HMM.

6 Numerical examples

In this section, we illustrate the performance of the RB-FE-HMM on three numerical examples related to various models (2.2),(2.4),(2.6) presented in Section 2. In the first example, we consider a stationary linear elliptic multiscale problem with a tensor displaying discontinuity on the micro sampling domains. The simulation of wave propagation in an imhomogeneous macro domain is treated in the second problem. In the last example, we consider a Richards equation (a nonlinear problem) in a 3D heterogeneous medium, a widely used model to evaluate the pressure head in soil infiltration models.

Computational settings. In the following numerical tests, we use a simplicial partition of the computational domain and piecewise linear polynomial basis functions. The quadrature points for the corresponding macro FEM are at the bary centers of the elements. All the tests are performed in a single thread Matlab environment, based on the code presented in [57]. The numerical convergence rates are presented in relative errors, e.g. $\frac{\|u^H - u^0\|}{\|u^0\|}$.

6.1 2D stationary problem with discontinuity on the micro domain

We consider in the macro domain $\Omega = [0,1]^2$ a stationary problem of the form,

$$-\nabla \cdot \big(a^\varepsilon(x)\nabla u^\varepsilon(x)\big) = f(x),\ x \in \Omega,$$

with a diagonal locoally periodic multiscale tensor with discontinuities illustrated in Fig. 2. We set $f(x) = 1$ and pose a mixed boundary condition, i.e. $u^\varepsilon(x) = 0,\ x \in \{x_1 = 0\} \cup \{x_1 = 1\}$, the normal derivative $\frac{\partial u^\varepsilon}{\partial n} = 0,\ x \in \{x_2 = 0\} \cup \{x_2 = 1\}$.

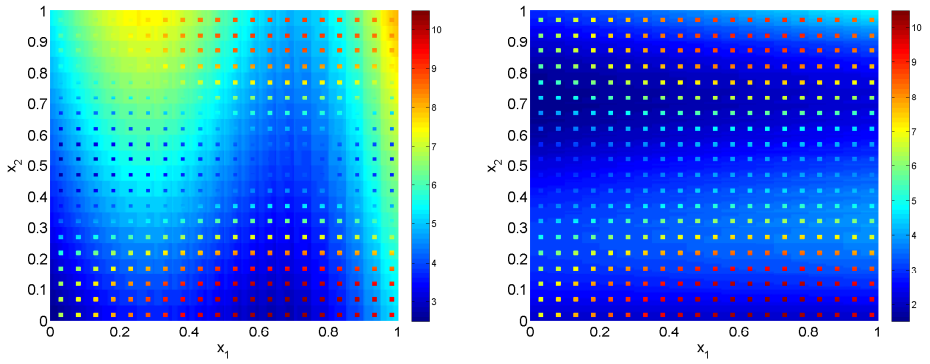

(a) $a^{\varepsilon}_{11}(x, x/\varepsilon)$ (b) $a^{\varepsilon}_{22}(x, x/\varepsilon)$

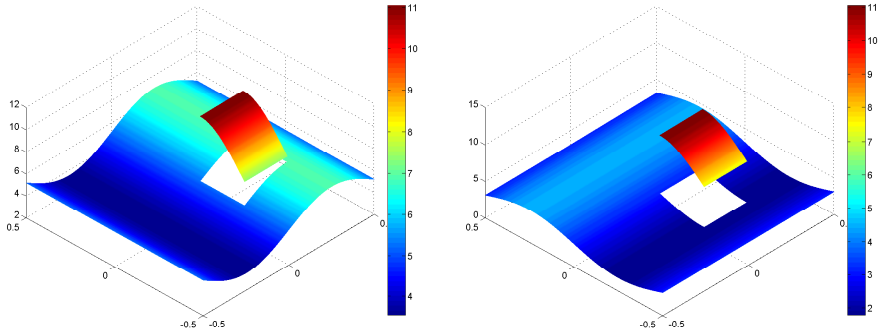

(c) $a^{\varepsilon}_{11}(\bar{x}, x/\varepsilon)$ (d) $a^{\varepsilon}_{22}(\bar{x}, x/\varepsilon)$

Fig. 2: Figure (a) and (b) illustrate the multiscale tensor in Ω with discontinuities where $\varepsilon = 0.05$. Figure (c) and (d) represent a zoom of the multiscale tensor on a cell $Y = \frac{x-\bar{x}}{\varepsilon}$ at macro location $\bar{x} = (0.5, 0.65)$.

Offline stage. We conduct the offline process following Algorithm 5.1. The offline settings and outputs are shown in Table 1. As can be seen that only 10 reduced basis functions are needed to reach our given precision tolerance 10^{-10}. At the end of the offline stage, necessary data (5.31), (5.33) are stored for later online use, as discussed in Section 5 (b). Due to the discontinuity of the affine representation in this example, we need to apply the so-called successive constraint method (SCM) [50] to estimate the coercive factor α.

Table 1: Offline settings and output for the discontinuous stationary problem.

Training set size	1000
Mesh	1000×1000
tol_{RB}	1e-10
RB Basis number	10
Offline CPU time	6149 s

Online stage. Next we apply the RB-FE-HMM online procedure to obtain the numerical homogenized solution $u^{H,RB}$. Here, we use uniform macro meshes with sizes $16 \times 16, 32 \times 32, 64 \times 64, 128 \times 128$ and 256×256, respectively. The values of the unknown homogenized tensor on the macro quadrature points are estimated using the RB obtained from the offline stage for any macro domain partition. In this test, we compare the RB-FE-HMM solution $u^{H,RB}$ with the FE-HMM solution as the reference solution for u^0 computed with a uniform 512×512 mesh as both macro and micro meshes. In Fig. 3 we show a loglog plot of the error $\|u^{H,RB} - u^0\|$ in the H^1 and L^2 norms versus $N_{mac} = M_{mac}^{1/d}$ where M_{mac} is the macroscopic DOF. According to the RB-FE-HMM a priori error analysis [27], the errors in the H^1 and L^2 norms decay with macro rates $\mathcal{O}(1/N_{mac})$ and $\mathcal{O}(1/N_{mac}^2)$ as confirmed by the numerical decay rates shown in Fig.3. As discussed in Section 5(b), the micro error e_{mic} of the RB-FE-HMM is $\mathcal{O}((\frac{h}{\varepsilon})^2)$ which is $\mathcal{O}(10^{-7})$ in our setting and remains unchanged during all the online procedures while the RB error e_{RB} is bounded by the given tolerance tol_{RB}. Therefore both e_{mic} and e_{RB} are negligible compared to e_{mac}.

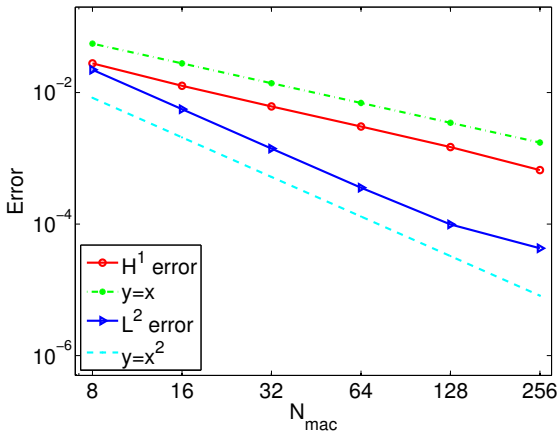

Fig. 3: The a priori errors $\|u^{H,RB} - u^0\|_{H^1(\Omega)}$ and $\|u^{H,RB} - u^0\|_{L^2(\Omega)}$ versus N_{mac} as we refine the macro mesh uniformly.

In Table 2, we present the CPU time comparison between the RB-FE-HMM and the

FE-HMM. As we can see when the macro meshsize reaches 256×256, the RB-FE-HMM online time is only 3% of the FE-HMM cost and even considering the offline overhead, the RB-FE-HMM is still more efficient than the FE-HMM. We conclude from this test that the RB-FE-HMM proceeds a significant computational speedup compared to the FE-HMM especially for relatively fine macro mesh.

Table 2: CPU time comparison between RB-FE-HMM and FE-HMM ($N_{mac} = N_{mic}$ for the FE-HMM). The offline CPU time is 6149 s.

Mesh	RB-FE-HMM Online CPU Time (s)	FE-HMM CPU Time (s)
8×8	0.05	0.15
16×16	0.13	0.99
32×32	0.51	12.3
64×64	2.1	195.6
128×128	8.0	3226.4
256×256	31.7	11112

6.2 Wave propagation in inhomogeneous media

In this example, we report numerical performance of the RB-FE-HMM for the linear multiscale wave equation (2.4). Here we consider a multiscale tensor that displays different heterogeneity in three subdomains as shown in Fig. 4 (a), where we marked each subdomain with one color and the multiscale tensor is diagonal and set as following,

$$a_{ii}^{\varepsilon} = \begin{cases} e^{-(x_1-0.15)^2-(x_2-0.85)^2} + 2.5(\cos(\pi x_2) + 1 + 2x_1)(\sin(2\pi x_i/\varepsilon) + 2) & x \in \Omega_1 \\ (\sin(6\pi x_1) + 2)^{-1} + (\cos(\pi x_2) + 1.1)(\sin(2\pi x_i/\varepsilon) + 2) & x \in \Omega_2 \\ 0.25(x_1^2 + x_2^2) + (3x_1 + 1.5x_2 + 0.3)(\sin(2\pi x_i/\varepsilon) + 2) & x \in \Omega_3 \end{cases}$$

We notice in Fig. 4 (b) that we have sharp media discontinuities across the different subdomain. We consider $u^{\varepsilon}(x, 0) = 0.1e^{-((x_1-1)^2+(x_2-1)^2)/\sigma^2}$, with $\sigma = 0.1$ as the initial condition and use zero Dirichlet boundary condition for simplicity.

Offline stage. Due to the different media, we perform the offline procedure in each subdomain and obtain three sets of offline basis functions which will be used in the online stage to estimate the unknown data in the corresponding subdomains. The offline settings and outputs for this test are presented in Table 3.

Table 3: Offline settings and output for the wave equation.

Subdomain	Ω_1	Ω_2	Ω_3
Training set size	1000	1000	1000
Micro mesh	1200×1200	1200×1200	1200×1200
tol_{RB}	1e-10	1e-10	1e-10
RB Basis number	10	8	6
Offline CPU time	954 s	786 s	620 s

Online stage. Using the offline outputs in the online procedure, we obtain the RB-FE-HMM solution u^{RB} shown in Fig. 5 (left pictures) at time $t = 0, 0.1$, and 0.2, respectively. For

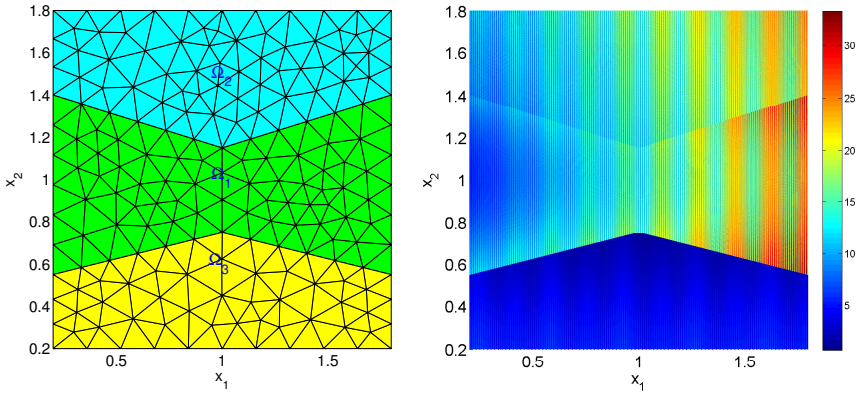

(a) Macro domain Ω (b) $a^{\varepsilon}_{11}(x)$ in Ω

Fig. 4: Heterogeneous medium with three different media having different wave speeds. Figure (a) shows the initial macro partition on Ω and Figure (b) shows the multiscale tensor a^{ε} in Ω for $\varepsilon = 0.05$.

the initial condition at time $t = 0$ we choose a Gaussian pulse. When the wave front reaches the subdomain Ω_3, a significant scattering occurs due to the small homogenized diffusion coefficient in Ω_3. We next compare our multiscale algorithm with a numerical solution by using the local arithmetic average of the multiscale tensor $a^{\varepsilon}(x)$ in each subdomain (see Fig. 5, right pictures). We can observe that the profiles of the two solutions differ significantly.

We finally compare the RB solution $u^{H,RB}$ to the standard FE solution obtained by solving the homogenized equation with the corresponding explicit homongenized tensor. The errors $\|\cdot\|_{L^\infty([0,T],L^2(\Omega))}$ and $\|\cdot\|_{L^\infty([0,T],H^1(\Omega))}$ are shown in Fig. 6. We can observe that the errors decay with rates $\mathcal{O}(1/N_{mac}^2)$ and $\mathcal{O}(1/N_{mac})$, which corroborates the analysis in [42].

6.3 Richards equation in an unsaturated soil domain

In the last example, we study a nonlinear parabolic multiscale problem similar to (2.6), known as the Richards equation in subsurface flow modeling. The classical Richards equation models the flow pressure head in an unsaturated media and is often combined with a mass transportation equation in order to simulate pollutants distribution in unsaturated soil [58]. In the literature on numerical simulations for Richards equation, the main study and experiments are usually done for single scale problems. However, the soil often has a multiscale structure due to the large scale range between the macro computational domain and the small pores structure in the soil. The solution of a 3D multiscale Richards equation is thus a challenging task, and we next discuss computational results obtained with the RB-FE-HMM.

We consider the following Richards equation in a 3D computational domain as presented in Fig. 7,

$$\frac{\Theta(u^{\varepsilon})}{\partial t} = \nabla \cdot \big(a^{\varepsilon}(x, u^{\varepsilon})\nabla u^{\varepsilon} - \mathbf{e}_3\big),$$

where u^{ε} is the pressure head of the pollutant flow and the water content function $\Theta(u)$ is

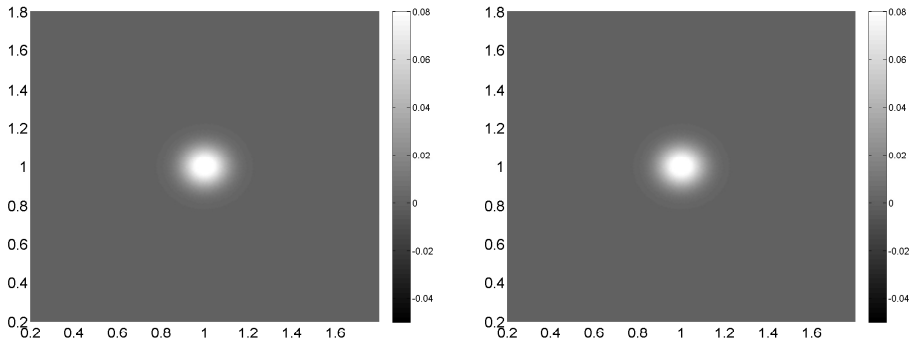

(a) $t = 0$

(b) $t = 0$

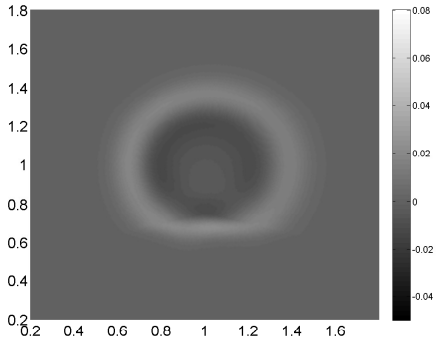

(c) $t = 0.1$

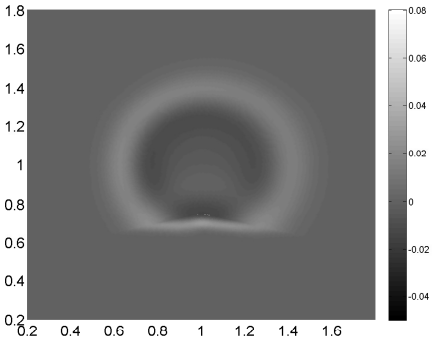

(d) $t = 0.1$

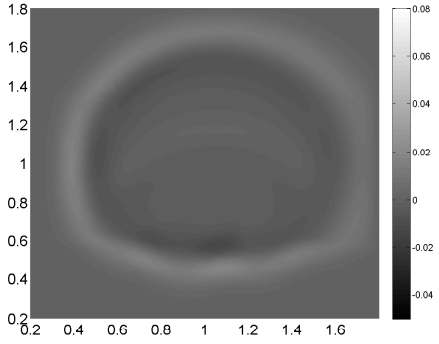

(e) $t = 0.2$

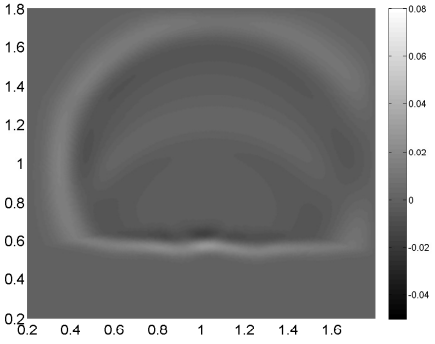

(f) $t = 0.2$

Fig. 5: The RB-FE-HMM solution $u^{H,RB}$ for problem (2.4) at time $t = 0, 0.1, 0.2$ (left figures), and FEM solution with arithmetic average of a^ε in the different subdomains (right figures).

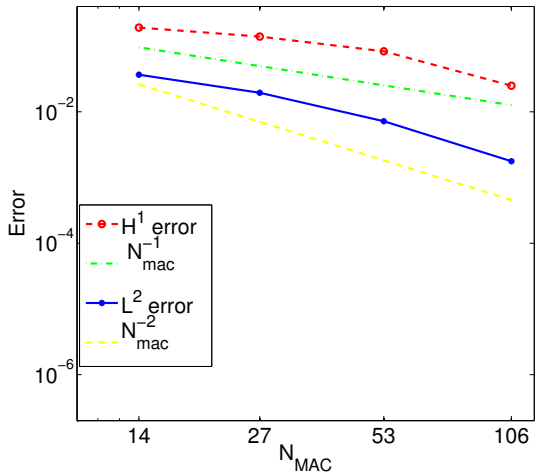

Fig. 6: H^1 and L^2 errors of $u^{H,RB}$ for the wave equation (2.4), where the reference solution u^0 is approximated by a single scale FEM using a resolved homogenized tensor.

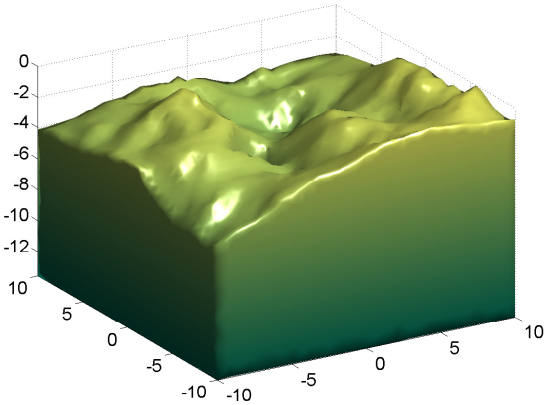

Fig. 7: The heterogeneous soil, modeled as the 3D macro computational domain Ω. We denote Ω_{Top} the rough surface on the top of the soil medium.

defined as

$$\Theta(u^\varepsilon) \quad = \quad \Theta_r + (\Theta_s - \Theta_r)(1 + |\alpha u^\varepsilon|^n)^{-m},$$

where the residual water content Θ_r, saturated water content Θ_s and α, n, m are model parameters shown in Table 4.

Table 4: Model parameter setting based on the numerical examples presented in [59].

Parameter	Test setting
Θ_r	0.368
Θ_s	0.102
n	2
m	$1 - 1/n$
α	-0.335

We next assume that the multiscale tensor is diagonal with entries defined as

$$a(x, u^\varepsilon)_{ii} \quad = \quad 5K(u^\varepsilon)K_s(x)\big(K_s(x) + K^\varepsilon_{s,i}(x)\big), \quad i = 1, 2, 3$$

where

$$\begin{aligned}
&K(u^\varepsilon) = ((1 + |\alpha u^\varepsilon|^n)^{-m})((1 + |\alpha u^\varepsilon|^n)^m - (|\alpha u^\varepsilon|^n)^m)^2,\\
&K_s(x) = 0.3\sin(x_1)\sin(x_2) + 0.8,\\
&K^\varepsilon_{s,i}(x) = (0.1\sqrt{|x_2|} + 0.5)(\sin(2\pi\frac{x_i}{\varepsilon}) + 2).
\end{aligned}$$

In order to show the variation of the pressure more clearly, we define the relative pressure head as $v^\varepsilon(x) = u^\varepsilon - x_3$ and therefore $v^\varepsilon(x)$ satisfies

$$\frac{\partial\Theta(v^\varepsilon + x_3)}{\partial t} = \nabla \cdot \big(a^\varepsilon(x; v^\varepsilon + x_3)\nabla v^\varepsilon(x)\big). \tag{6.35}$$

We assume that the initial condition is $v^\varepsilon(x, 0) = 0.1x_3 - 0.5$ and that on the top boundary $\partial\Omega_{Top}$ of the domain Ω v^ε satisfies Dirichlet boundary condition $v^\varepsilon(x, t) = 0.1x_3 - 0.5,\ x \in \partial\Omega_{Top}$. Homogeneous Neumann boundary condition are set on all the other boundaries. Homogenization for such problems has been studied in [60], where it is shown that the homogenized Richards equation has the same form as (6.35) with an oscillating tensor replaced by a homogenized one.

Offline stage. As mentioned in Section 5(a), for this type of nonlinear problems we have cell problems defined in (5.27) indexed by parameter $\tau = \kappa, m$ where $\kappa = (x, s)$. We apply the RB-FE-HMM technique to (5.29) with $\kappa = (x, s)$. The offline settings and outputs can be seen in Table 5, where the parameter range of s is estimated by an offline procedure proposed in [61].

Online stage. The total evolution time we consider in this experiment is $t = 3$ and we set the time step $\Delta t = 0.005$ for the time integrator. We use the linearized Picard scheme proposed in [62] and a macro mesh with 12304 DOF. The total RB-FE-HMM online computational time is $4197s$ for 600 time steps and for each time step the CPU time cost is about $6.5s$. As for the CPU time comparison, we performed a computation with single scale FEM with the same macro mesh, for which each time step computation took around $2s$. Therefore we can conclude that the RB-FE-HMM online time cost is comparable to a single scale FEM (up to some constant). In Fig. 8, we show the evolution of $v^0(x, t)$ from $t = 0$ to the final time $t = 3$, illustrating the variation of the pressure head in the soil domain.

Table 5: Offline settings and outputs for Richards equation.

Parameter domain	$\Omega \times [-2, 0.5]$
Training set size	5000
Solver DOF	8 000 000
tol_{RB}	1e-10
RB Basis number	12

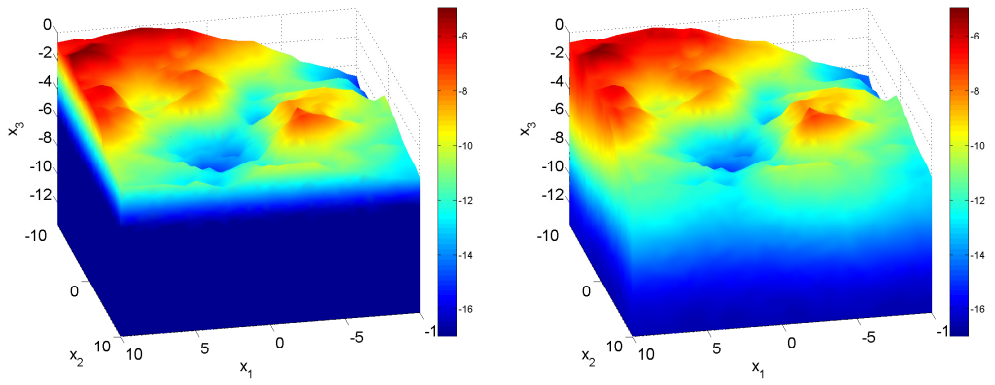

(a) $t = 0$ (b) $t = 3$

Fig. 8: The solution $v^0(x, t)$ at initial $t = 0$ and final time $t = 3$.

7 Conclusion

We have presented a unified framework to combine reduced order modeling techniques with numerical homogenization methods for a variety of problems including linear and nonlinear elliptic, parabolic and wave equations with highly oscillatory data. The reduced order modeling technique, built on the reduced basis method, allows to precompute a representative number of micro functions in an offline stage. This precomputed reduced basis is then used in an online stage to compute effective data for a homogenized model at arbitrary locations in the computational domain. The use of reduced basis also allows the outputs of the offline stage to be repeatedly used for many-query contexts. The accuracy of this representative basis is controlled by appropriate a posteriori error estimators in the offline stage that also permit to certify the accuracy of the online solution. We have shown that two issues in the numerical approximation of PDEs with multiple scales are addressed by the RB-FE-HMM, namely

- a computational cost *independent* of the size of the oscillatory parameter ε thanks to the numerical homogenization techniques,
- a linear computational cost for the online stage obtained through the reduced basis available for the online micro problems.

Finally, we have tested the numerical method on a variety of problems, including an elliptic problem with discontinuous microscopic oscillatory data, wave propagation in inhomogeneous media, and a three-dimensional infiltration problem in an unsaturated porous media. Sub-

stantial computational saving are observed for the new reduced order modeling numerical homogenization method when compared to classical numerical homogenization.

Acknowledgment

The research of A. A. and Y. B. is partially supported by the Swiss National Foundation 200021_134716.

References

[1] I. Babuška, Homogenization and its application. Mathematical and computational problems, Numerical solution of partial differential equations, III (Proc. Third Sympos. (SYNSPADE), Univ. Maryland, College Park, Md., 1975) (1976) 89–116.

[2] A. Bensoussan, J.-L. Lions, G. Papanicolaou, Asymptotic analysis for periodic structures, North-Holland Publishing Co., Amsterdam, 1978.

[3] G. Nguetseng, A general convergence result for a functional related to the theory of homogenization, SIAM J. Math. Anal. 20 (3) (1989) 608–623.

[4] G. Allaire, Homogenization and two-scale convergence, SIAM J. Math. Anal. 23 (6) (1992) 1482–1518.

[5] V. Jikov, S. Kozlov, O. Oleinik, Homogenization of differential operators and integral functionals, Springer-Verlag, Berlin, Heidelberg, 1994.

[6] F. Murat, L. Tartar, H-convergence, topics in the mathematical modeling of composite materials, Progr. Nonlinear Differential Equations Appl. 31 (1997) 21–43.

[7] S. Torquato, Random Heterogeneous Materials, Vol. 16, Springer, IAM, 2005.

[8] I. Babuska, J. Osborn, Generalized finite element methods: their performance and their relation to mixed methods, SIAM J. Numer. Anal. 20 (1983) 510–536.

[9] T. Hou, X. Wu, Z. Cai, Convergence of a multiscale finite element method for elliptic problems with rapidly oscillating coefficients, Math. Comp. 68 (227) (1999) 913–943.

[10] J. Alcock, K. Burrage, A note on the balanced method, BIT 46 (4) (2006) 689–710.

[11] H. Owhadi, L. Zhang, Localized bases for finite-dimensional homogenization approximations with nonseparated scales and high contrast, Multiscale Model. Simul. 9 (4) (2011) 1373–1398. doi:10.1137/100813968.

[12] Y. Efendiev, T. Y. Hou, Multiscale finite element methods. Theory and applications, Vol. 4 of Surveys and Tutorials in the Applied Mathematical Sciences, Springer, New york, 2009.

[13] T. J. R. Hughes, Multiscale phenomena: Green's functions, the Dirichlet-to-Neumann formulation, subgrid scale models, bubbles and the origins of stabilized methods, Comput. Methods Appl. Mech. Engrg. 127 (1-4) (1995) 387–401. doi:10.1016/0045-7825(95)00844-9.

[14] F. Brezzi, A. Russo, Choosing bubbles for advection-diffusion problems, Math. Models Methods Appl. Sci. 4 (4) (1994) 571–587. doi:10.1142/S0218202594000327.

[15] G. Sangalli, Capturing small scales in elliptic problems using a residual-free bubbles finite element method, Multiscale Model. Simul. 1 (3) (2003) 485–503 (electronic). doi:10.1137/S1540345902411402.

[16] G. Allaire, M. Briane, Multiscale convergence and reiterated homogenisation, Proc. Roy. Soc. Edinburgh Sect. A 126 (2) (1996) 297–342.

[17] A.-M. Matache, C. Schwab, Two-scale fem for homogenization problems, M2AN Math. Model. Numer. Anal 36 (4) (2002) 537–572.

[18] V. H. Hoang, christoph Schwab, High-dimensional finite elements for elliptic problems with multiple scales, Multiscale Model. Simul 3 (1) (2005) 168–194.

[19] M. E. Brewster, G. Beylkin, A multiresolution strategy for numerical homogenization, Appl. Comput. Harmon. Anal. 2 (4) (1995) 327–349. doi:10.1006/acha.1995.1024.

[20] B. Engquist, O. Runborg, Wavelet-based numerical homogenization with applications, Multiscale and multiresolution methods 20 (2002) 97–148.

[21] W. E, B. Engquist, The heterogeneous multiscale methods, Commun. Math. Sci. 1 (1) (2003) 87–132.

[22] A. Abdulle, W. E, B. Engquist, E. Vanden-Eijnden, The heterogeneous multiscale method, Acta Numer. 21 (2012) 1–87.

[23] C. J. Feyel F, Fe2 multiscale approach for modelling the elastoviscoplastic behaviour of long fibre SiC/Ti, composite materials, Comput. Methods Appl. Mech. Engrg. 183 (2000) 309–330.

[24] K. Terada, N. Kikuchi, A class of general algorithms for multi-scale analyses of heterogeneous media, Comput. Methods Appl. Mech. Engrg. 190 (40-41) (2001) 5427–5464.

[25] C. Miehe, J. Schröder, C. Bayreuther, On the homogenization analysis of composite materials based on discretized fluctuations on the micro-structure, Acta Mechanica 135 (2002) 1–16.

[26] Q. Yu, J. Fish, Multiscale asymptotic homogenization for multiphysics problems with multiple spatial and temporal scales: a coupled thermo-viscoelastic example problem, Internat. J. Solids Structures 39 (26) (2002) 6429–6452.

[27] A. Abdulle, Y. Bai, Reduced basis finite element heterogeneous multiscale method for high-order discretizations of elliptic homogenization problems, J. Comput. Phys. 231 (21) (2012) 7014–7036.

[28] A. Abdulle, Y. Bai, Adaptive reduced basis finite element heterogeneous multiscale method, Comput. Methods Appl. Mech. Engrg. 257 (2013) 201–220.

[29] A. Abdulle, Y. Bai, G. Vilmart, Reduced basis finite element heterogeneous multiscale method for quasilinear elliptic homogenization problems, Discrete Contin. Dyn. Syst.

[30] L. Tartar, Estimations des coefficients homogénéisés, Lectures Notes in Mathematics 704, Springer-Verlag, Berlin, 1977.

[31] A.Pankov, G convergence and homogenization of nonlinear partial differential operators, Springer Seriesin Mathematics and Its Applications 422, Springer Science+Business Media Dordrecht, Netherlands, 1997.

[32] D. Cioranescu, P. Donato, An introduction to homogenization., Vol. 17 of Oxford Lecture Series in Mathematics and its Applications, Oxford University Press, New York, 1999.

[33] A. Abdulle, On a priori error analysis of fully discrete heterogeneous multiscale FEM, SIAM, Multiscale Model. Simul. 4 (2) (2005) 447–459.

[34] W. E, P. Ming, P. Zhang, Analysis of the heterogeneous multiscale method for elliptic homogenization problems, J. Amer. Math. Soc. 18 (1) (2005) 121–156.

[35] A. Abdulle, Discontinuous galerkin finite element heterogeneous multiscale method for elliptic problems with multiple scales, Math. Comp. 81 (278) (2012) 687–713.

[36] A. Abdulle, M. Huber, Discontinuous galerkin finite element heterogeneous multiscale method for advection-diffusion problems with multiple scales, To appear in Numer. Math.

[37] P. Ciarlet, P. Raviart, The combined effect of curved boundaries and numerical integration in isoparametric finite element methods, Math. Foundation of the FEM with Applications to PDE (1972) 409–474.

[38] A. Abdulle, The finite element heterogeneous multiscale method: a computational strategy for multiscale PDEs, Vol. 31 of Gakuto Internat. Ser., Math. Sci. Appl., Gakkotosho Co. Ltd., Tokyo, 2009.

[39] A. Abdulle, A priori and a posteriori error analysis for numerical homogenization: a unified framework, Ser. Contemp. Appl. Math. CAM 16 (2011) 280–305.

[40] A. Abdulle, G. Vilmart, The effect of numerical integration in the finite element method for nonmonotone nonlinear elliptic problems with application to numerical homogenization methods, C. R. Acad. Sci. Paris, Ser. I 349 (19-20) (2011) 1041–1046.

[41] A. Abdulle, G. Vilmart, Analysis of the finite element heterogeneous multiscale method for quasilinear elliptic homogenization problems, Math. Comp. 83 (286) (2014) 513–536. doi:10.1090/S0025-5718-2013-02758-5.

[42] A. Abdulle, M. Grote, Finite element heterogeneous multiscale method for the wave equation, SIAM, Multiscale Model. Simul. 9 (2) (2011) 766–792.

[43] A. Abdulle, G. Vilmart, Coupling heterogeneous multiscale FEM with Runge-Kutta methods for parabolic homogenization problems: a fully discrete space-time analysis, Math. Models Methods Appl. Sci. 22 (6) (2012) 1250002/1–1250002/40.

[44] J. T. Oden, K. S. Vemaganti, Estimation of local modeling error and goal-oriented adaptive modeling of heterogeneous materials. I. Error estimates and adaptive algorithms, J. Comput. Phys. 164 (1) (2000) 22–47.

[45] L. Boccardo, F. Murat, Homogénéisation de problèmes quasi-linéaires, Publ. IRMA, Lille 3 (7) (1981) 13–51.

[46] R. Du, P. Ming, Heterogeneous multiscale finite element method with novel numerical integration schemes, Commm. Math. Sci. 8 (4) (2010) 863–885.

[47] A. Abdulle, B. Engquist, Finite element heterogeneous multiscale methods with near optimal computational complexity, SIAM, Multiscale Model. Simul. 6 (4) (2007) 1059–1084.

[48] A. Abdulle, A. Nonnenmacher, Adaptive finite element heterogeneous multiscale method for homogenization problems, Comput. Methods Appl. Mech. Engrg. 200 (37-40) (2011) 2710–2726.

[49] C. Prud'homme, D. V. Rovas, K. Veroy, L. Machiels, Y. Maday, A. T. Patera, G. Turinici, Reliable real-time solution of parametrized partial differential equations: Reduced-basis output bounds methods, J. Fluids Eng. 124 (2002) 70–80.

[50] A. T. Patera, G. Rozza, Reduced Basis Approximation and A Posteriori Error Estimation for Parametrized Partial Differential Equations, to appear in (tentative rubric) MIT Pappalardo Graduate Monographs in Mechanical Engineering, 2007.

[51] G. Rozza, D. Huynh, A. T. Patera, Reduced basis approximation and a posteriori error estimation for affinely parametrized elliptic coercive partial differential equations, Arch. Comput. Methods. Eng. 15 (2008) 229–275.

[52] S. Boyaval, Reduced-basis approach for homogenization beyond the periodic setting, Multiscale Model. Simul. 7 (1) (2008) 466–494.

[53] S. Boyaval, Mathematical modeling and simulation for material science, PhD thesis, University Paris Est, 2009.

[54] M. Barrault, Y. Maday, N. Nguyen, A. Patera, An 'empirical interpolation method': Application to efficient reduced-basis discretization of partial differential equations, C. R. Acad. Sci. Paris Ser.I 339 (2004) 667–672.

[55] A. Buffa, Y. Maday, A. T. Patera, C. Prud'homme, G. Turinici, A priori convergence of the greedy algorithm for the parametrized reduced basis, ESAIM: M2AN 46 (2012) 595–603.

[56] P. Binev, A. Cohen, W. Dahmen, R. Devore, G. Petrova, P. Wojtaszczyk, Convergence rates for greedy algorithms in reduced basis methods, SIAM J. Math. Anal. 43 (2011) 1457–1472.

[57] A. Abdulle, A. Nonnenmacher, A short and versatile finite element multiscale code for homogenization problem, Comput. Methods Appl. Mech. Engrg 198 (37-40) (2009) 2839–2859.

[58] F. Botros, Y. Onsoy, T. Ginn, T. Harter, Richards equation-based modeling to estimate flow and nitrate transport in a deep alluvial vadose zone, Vadose Zone J.

[59] M. Celia, E. Bouloutas, R. Zarba, A general mass-conservative numerical solution for the unsaturated flow equation, Water Resources Research 26 (7) (1990) 1483–1496.

[60] P. Heuser, Homogenization of quasilinear elliptic-parabolic equations with respect to measures, Inaugural Dissertation, Naturwissenschaftlich-Mathematischen der Gesamtfakultaet der Ruprecht-Karls-Universitaet Heidelberg, 2008.

[61] A. Abdulle, Y. Bai, G. Vilmart, An online-offline homogenization strategy to solve quasilinear two-scale problems at the cost of one-scale problems, Submitted.

[62] C. Paniconi, A. Aldama, E. Wood, Numerial evaluation of iterative and noniterative methods for the solution of the nonlinear richards equation, Water resources reasearch 29 (4) (1991) 1147–1163.